J MATER SCI **41** (2006) 1029–1037

Synthesis and characterization of coprecipitation-derived ferrimagnetic glass-ceramic

O. BRETCANU, S. SPRIANO, C. BROVARONE VITALE, E. VERNÉ
Materials Science and Chemical Engineering Department, Politecnico di Torino, Italy
E-mail: oana.bretcanu@polito.it

Published online: 4 February 2006

Ferrimagnetic glass-ceramics could be used for magnetic induction hyperthermia. This technique is utilised for the destruction of solid neoplastic diseases by application of an alternating magnetic field. Biocompatible ferrimagnetic materials could be easily incorporated into a tumour and could generate heat mainly by hysteresis loss.

A ferrimagnetic glass-ceramic in the system SiO_2–Na_2O–CaO–P_2O_5–FeO–Fe_2O_3 has been prepared by melting of the coprecipitation-derived raw materials. This glass-ceramic contains a unique crystalline phase, magnetite, embedded in an amorphous matrix. Magnetite crystals precipitate during cooling from melting temperature. This glass-ceramic would no longer require any nucleation and growth thermal treatment, since the maximal quantity of magnetite crystals was produced during cooling. The average unit-cell parameter, crystallite size of magnetite, and the quantitative ratio of the crystallographic phases in the glass-ceramic samples were evaluated using two different methods. Similar results were obtained with both methods. The magnetite crystals are about 50 nm in dimensions. The samples contain 45 wt% of magnetite, homogeneously distributed in the amorphous residual matrix.

The as prepared glass-ceramic has a saturation magnetisation of 34 $A{\cdot}m^2/kg$ and a coercive force of 6.7 kA/m. The estimated magnetic loss/cycle under the magnetic field up to 796 kA/m is around 1.45 mJ/g. The specific power loss of this glass-ceramic under a magnetic field of 40 kA/m and a frequency of 440 kHz is 25 W/g.

This material showed a bioactive behaviour, as after 2 weeks of soaking in a simulated body fluid the formation of a hydroxylapatite layer on their surface was observed. This feature makes it also suitable for bone cancer.

1. Introduction

One of the procedures proposed for cancer therapy is hyperthermia, i.e. the exposition of body tissue to high temperatures (up to 100°C). Hyperthermia is almost always joined to other forms of cancer therapy (radiation therapy, chemotherapy and biological therapy) in order to increase their effectiveness.

The blood flow in normal tissues vastly increases during heating up to temperatures commonly used in clinical hyperthermia (41–45°C). This increase in blood flow effectively dissipates the heat during hyperthermic application. In contrast, at 41–42°C, in most of the tumours, vascular occlusion, stasis and haemorrhage can occur [1]. The heat dissipation in the tumours is poor, particularly in the large tumours, due to the decrease in blood flow and vascular damage. Consequently, hyperthermia preferentially heats and causes greater damage in tumours than in normal tissues. Hyperthermia also selectively decreases pH in tumours, which appears to be related to the vascular occlusion. This decrease in pH, joined to depletion of nutrients, including oxygen, not only enhance the heat sensitivity of tumour cells, but also inhibit the recovery of tumour cells from heat damage and provoke further cell death after heat application. Furthermore, the hostile environment in the heated tumours appears to suppress the development of thermo-tolerance [1].

Magnetic induction is one of available forms of inducing deep-regional hyperthermia. When a magnetic material is subjected to an oscillating magnetic field, it can generate heat due to magnetic hysteresis loss. The amount of heat generated per cycle depends on the nature of ferrimagnetic material and of magnetic field parameters. Magnetic particles embedded around a tumour site and placed within an oscillating magnetic

0022-2461
DOI: 10.1007/s10853-005-2636-x

field will heat up to a temperature dependent on the magnetic properties of the material, the strength of the magnetic field, the frequency of oscillation and the cooling capacity of the blood flow in the tumour site [2].

Several materials presenting the ability of generating heat by hysteresis loss have been developed. Bioactive and ferrimagnetic glass-ceramics are expected to be useful as thermo-seeds for hyperthermia treatment of bone tumours. When they are implanted in proximity of the tumours, they could destroy cancer cells by indirect heating (due to the ferrimagnetic properties) and also could form an interfacial bond with bone (due to the bioactivity behaviour). *In vitro* and *in vivo* tests demonstrate that bioactive implant materials form a layer of biologically active hydroxyl carbonate apatite on the implant surface [3]. For this reason, bioactive glass-ceramics can stably fixed around the tumours and reinforce the weakened bone by chemical bonding.

Thus, these materials could be successfully used not only for tumour destruction, but also as bone substitutes. For example, after surgical resection by curettage of invasive and relapsing benign tumours, the glass-ceramic could be implanted and repetitive hyperthermic treatments could be applied. Therefore, these materials could be implanted once and then successive cyclic cancer treatments could be performed.

A number of authors reported the synthesis of ferrimagnetic glass-ceramics in the systems SiO_2–CaO–Fe_2O_3, SiO_2–CaO–Fe_2O_3–B_2O_3–P_2O_5 or SiO_2–Al_2O_3–Fe_2O_3–P_2O_5–Li_2O by controlled crystallisation [4–9].

In this study, we have synthesised a ferrimagnetic glass-ceramic belonging to the system SiO_2–Na_2O–CaO–P_2O_5–FeO–Fe_2O_3, by melting of the coprecipitated starting materials. The structure and the properties of this glass-ceramic have been analysed by X-ray diffraction (XRD), scanning electron microscopy (SEM), energy dispersive spectroscopy (EDS), transmission electron microscopy (TEM), vibrating sample magnetometer (VSM) and *in vitro* tests. In order to estimate the heat generation of these materials, calorimetric measurements have also been performed.

2. Materials and methods

2.1. Sample preparation

The composition of the ferrimagnetic glass-ceramic prepared in this work is: $24.7SiO_2$–$13.5Na_2O$–$13.5CaO$–$3.3P_2O_5$–$14FeO$–$31Fe_2O_3$ (wt%). This glass-ceramic is denominated generically S45 because the sum of the weight percents of iron oxides is 45. The raw materials utilised for the preparation of this glass-ceramic were obtained by coprecipitation from aqueous soluble salts solutions [10, 11]. The starting reagents are water soluble salts: $NaNO_3$, $Ca(NO_3)_2{\cdot}4H_2O$, $(NH_4)_2HPO_4$, $FeSO_4{\cdot}7H_2O$, $Fe(NH_4)(SO_4)_2{\cdot}12H_2O$ and colloidal SiO_2, which coprecipitate in a basic medium of NH_4OH. Each reagent (except for colloidal SiO_2 solution) was dissolved separately into a minimum quantity of distillate water using a heating magnetic stirrer. The reagents solutions were then intimately mixed together, and the coprecipitation occurred immediately. During the coprecipitation, the obtained sol was stirred with a medium speed, and the pH was maintained around 9–10 using NH_4OH solution. After the addition of NH_4OH the precipitate becomes dark green, almost black. The precipitate was kept in a reaction recipient (beaker) at room temperature for 1 day. Then the resulting precipitate was washed 3 times with distillate water and filtered. The obtained powder was then dried at 150°C in oven.

The dried powder was milled in a ball mill for 30 min and then was thermally treated for decomposition into a furnace, in air, up to 900°C using a heating rate of 10°C/min and a dwell time of 3 h. After heating, the resulted powder was crushed in a mortar in order to deagglomerate the particles and then melted in a platinum crucible at 1500°C 30 min under air atmosphere. After then, the melt was poured on a copper plate at room temperature, obtaining the glass-ceramic.

After cooling, a part of the glass-ceramic S45 was milled down to a size smaller than 45 μm and the other part was cut into small pieces $5 \times 5 \times 2$ mm^3, polished with SiC paper and washed with distillate water in an ultrasonic cleaner.

2.2. X-ray diffraction

X-ray diffraction (XRD) patterns were registered by a Philips X`Pert diffractometer with Cu K_α radiation. Diffraction patterns were detected by using a step of 0.02° (2θ) with a fixed counting time of 15 s per step. The phase identification as well as the determination of crystallite size and lattice constant was performed by profile fitting of each diffraction peak. The "X'Pert HighScore" program, with PCPDFWIN database (2002 JCPDS — International Centre for Diffraction Data) was employed.

The values of crystallite sizes of magnetite were calculated by using the Scherrer formula [12]. The values of lattice constant a_0 of the magnetite were calculated from experimental interplanar spacing for each diffraction peak. In order to eliminate the systematic errors such as sample absorption and divergence of the beam, the average value of the lattice constant was extrapolated linearly to $F\ (2\theta) = 0$, by using the Taylor and Sinclair method [12], as the major part of the peaks lies between $2\theta = 30$–$90°$.

Quantitative analysis was performed by application of the internal standard method proposed by Klug and Alexander [12]. The contents of the magnetite crystallised in the specimens were determined from the calibration curve using fluorite (CaF_2) as internal standard. Synthetic mixtures of completely amorphous phase and 25, 50, 75 and 100 wt% of pure magnetite in powder form (Aldrich, 98% purity, grain size <5 μm) were each admixed with fluorite in the constant proportion of 20 wt%. The completely amorphous phase was obtained by melting at 1650°C the crushed powders obtained after heat

treatment at 900°C (prepared as described before) and rapid quenching it in water. Then, the same fraction of fluorite (20 wt%) was added to the investigated samples of glass-ceramic and all the mixtures were analysed by XRD. The obtained diffraction data patterns of the mixtures were fitted and the intensity ratio between the (311) magnetite diffraction line and (111) fluorite line was determined and plotted against the weight fraction of magnetite. Each plotted point of the calibration curve is the average of three determinations.

The second method utilised for quantitative analysis was the MAUD program. This program is based on the Rietveld method [13]. The amorphous phase structure was approximated by considering it as silica where the long-range order is lost and a crystallite size is about one cell [14–16]. The nanocrystalline model of silica glass phase reported in this software was refined in order to obtain a good fitting for our structure. For the quantitative analysis, the completely amorphous phase (prepared as described above) and pure magnetite powder (Aldrich) were used as references in order to determine the scale factor.

2.3. Scanning electron microscopy

Scanning electron microscopy (SEM) was performed in a Philips 515 coupled with energy dispersive spectroscopy (EDS) EDAX PV 9900. In order to analyse the crystals morphology, polished glass-ceramic samples were chemically treated with a solution of 5% volume of HF:HNO_3 in a molar ratio 1:1 for 1 min, washed with distilled water, dried at room temperature and observed by SEM.

2.4. Transmission electron microscopy

Transmission electron microscopy (TEM) was carried out with CM12/STEM Electron Microscope PW 6030 Philips at 120 kV. The powder samples were suspended in isopropanol using an ultrasonic cleaner. A few drops of the suspension were placed on microgrids (copper grids coated with thin carbon film, 200 mesh) and then let to dry at room temperature. For magnetite identification, the electron diffraction (ED) patterns were analysed [17]. TEM camera diffraction constant was assessed on a pure aluminium standard sample.

2.5. Magnetic measurements

The magnetic properties were measured using a vibrating sample magnetometer (VSM) with a maximum applied field of 1.4 MA/m (17 kOe), at room temperature, in static conditions. The calibration curve was made using a nickel sphere as a standard reference material, with a saturation magnetisation of 3.56 mA·m^2 (3.56 emu), positioned in the centre of the pick-up coils.

The magnetic hysteresis cycle of glass-ceramic and pure magnetite were measured using an applied field of 796 kA/m (10 kOe), 39.8 kA/m (500 Oe) and 4.8 kA/m (60 Oe). Pure magnetite particles (Aldrich, 98% purity, grain size <5 μm) were used as reference.

2.6. Calorimetric measurements

Calorimetric measurements were performed using a magnetic induction furnace, with a magnetic field intensity of 40 kA/m (≅500 Oe) and 440 kHz frequency. Small pieces of glass-ceramic S45 were immersed in 20 ml water in a plastic container, which was then placed in the centre of the coil. The alternating magnetic field was applied for 2 min. Right after the power was switched off, the container was shaken to equilibrate the water temperature. The water temperature before and after the application of magnetic field was measured with a thermocouple. The sample's weight (0.05–0.1 g) was much smaller than the water's mass (20 g) and the heat absorbed by the sample was neglected.

2.7. Bioactivity test

In vitro bioactivity test was carried out by soaking the glass-ceramic pieces (5 × 5 × 2 mm^3) in 15 ml simulated body fluid (SBF) (proposed by Kokubo *et al.* [18]) at 37°C in polyethylene containers. The composition of the SBF solution is given in Table I. The pH of the SBF solution was buffered at 7.40 before soaking. The SBF solution was refreshed twice a week. After soaking, the specimens were removed from the fluid and gently washed with distilled water. After drying in air atmosphere, the surface of the samples was observed by SEM in order to assess their bioactivity by detecting the formation of hydroxylapatite on their surfaces.

3. Results and discussion

In the present study, a bioactive and ferrimagnetic glass-ceramic in the system SiO_2–Na_2O–CaO–P_2O_5–FeO–Fe_2O_3 has been prepared by a coprecipitation-derived method. Traditionally, the aim of coprecipitation is to obtain very fine crystalline phases in order to prepare multicomponent ceramic oxides through the formation of an intermediate precipitate, usually hydrous oxides in an aqueous medium. The components are mixed at the colloidal or molecular scale so they have a very good chemical homogeneity [19, 20]. This effect

TABLE I Ion concentrations (mM) of SBF and human blood plasma

Ion	SBF	Blood plasma
Na^+	142.0	142.0
K^+	5.0	5.0
Mg^{2+}	1.5	1.5
Ca^{2+}	2.5	2.5
Cl^-	147.8	103.0
HCO_3^-	4.2	27.0
HPO_4^{2-}	1.0	1.0
SO_4^{2-}	0.5	0.5

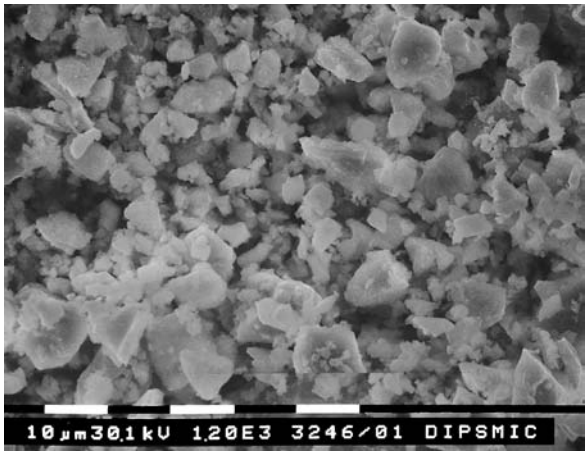

Figure 1 SEM micrograph of glass-ceramic S45 after grinding and sieving.

usually confers to the obtained powders a high degree of homogeneity, strong reactivity, high purity and lower processing temperatures if compared with traditional ceramics. In this case, the goal was to obtain a glass-ceramic rather than a ceramic material, so a melting step was still necessary, in order to achieve the nucleation of magnetite in a liquid-derived amorphous phase. The preparation of the starting powders by coprecipitation brought some advantages in respect to the conventional melting of commercial reagents, such as better homogeneity (molecular scale) and enhanced purity of the raw materials.

The morphology of the glass-ceramic particles obtained by grinding and sieving is presented in Fig. 1. It can be observed that the particles have a typical shape of crushed materials with sharp edges and corners. The grains size varies from few microns to 20 μm.

3.1. X-ray diffraction

Fig. 2 shows the X-ray diffraction patterns performed on this glass-ceramic powder. A characteristic amorphous halo can be observed in the range $2\theta = 20$–$35°$. The unique crystalline phase identified is magnetite (Fe_3O_4). The reflections related to magnetite are very well defined and are identified using ($h\,k\,l$) planes index. Therefore, by using this derived coprecipitation method, we observed a glass-ceramic material presenting a unique crystalline phase, magnetite, as shown by XRD diffraction patterns (Fig. 2). Magnetite crystals form during cooling from melting temperature of 1500°C, without any successive crystallisation treatment.

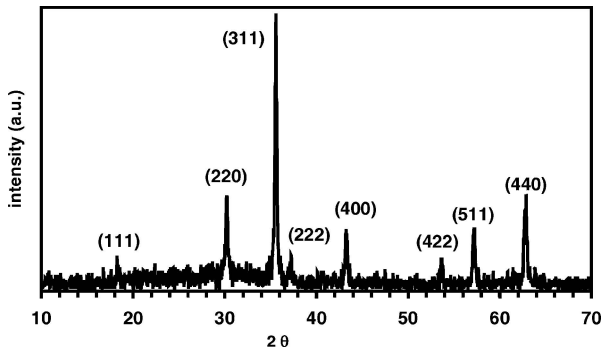

Figure 2 XRD patterns of glass-ceramic S45 ((*hkl*) = magnetite).

The values of crystallites dimension perpendicular to the crystallographic planes, calculated from the broadening of each diffraction peak are presented in Table II. An average crystal size of 53 ± 9 nm was estimated.

The values of unit-cell parameter a_0 of the crystallised magnetite and of the parameter F (2θ) are shown in Table III and Table IV, respectively. The linear fitting curve of variation of a_0 in function of F (2θ) was plotted in Fig. 3. The correlation coefficient $R = 0.99925$ and the standard deviation SD = 3.06054 E-4, indicate a very good fitting. By using the linear extrapolation to F (2θ) = 0, the lattice parameter of crystallised magnetite presented in the glass-ceramic sample is $a_0 = 8{,}4013$ Å.

TABLE II Calculation of the crystals size of magnetite from the diffraction maxima profiles of glass-ceramic S45

No.	Peak position 2θ (°)	cos θ (radians)	tan θ (radians)	Line broadening β (°)	Crystals size d (nm)
1	18.22	0.987	0.160	0.1315	61.24
2	30.02	0.966	0.268	0.1377	59.78
3	35.40	0.953	0.319	0.1564	53.37
4	37.00	0.948	0.335	0.1183	70.88
5	42.99	0.930	0.394	0.1866	45.80
6	53.36	0.894	0.502	0.1998	44.54
7	56.88	0.879	0.542	0.212	42.66
8	62.47	0.855	0.606	0.2005	46.38

TABLE III Calculation of the lattice constant a_0 of the magnetite from the diffraction pattern of glass-ceramic S45

No.	2θ (°)	h	k	l	$\sqrt{m}$	d_{hkl}(Å)	a_0(Å)
1	18.22	1	1	1	1.73	4.86	8.426
2	30.02	2	2	0	2.83	2.97	8.414
3	35.40	3	1	1	3.32	2.54	8.411
4	37.00	2	2	2	3.46	2.43	8.410
5	42.99	4	0	0	4.00	2.10	8.408
6	53.36	4	2	2	4.90	1.72	8.405
7	56.88	5	1	1	5.20	1.62	8.404
8	62.47	4	4	0	5.66	1.49	8.404

TABLE IV Calculation of the function F (2θ) for the extrapolation of the lattice constant of glass-ceramic S45

No.	2θ (°)	2θ (radians)	sin (2θ)	$\cos^2(2\theta)$	F (2θ)
1	18.22	0.32	0.31	0.90	5.72
2	30.02	0.52	0.50	0.75	2.93
3	35.40	0.62	0.58	0.66	2.23
4	37.00	0.65	0.60	0.64	2.05
5	42.99	0.75	0.68	0.53	1.5
6	53.36	0.93	0.80	0.36	0.83
7	56.88	0.99	0.84	0.30	0.66
8	62.47	1.09	0.89	0.21	0.44

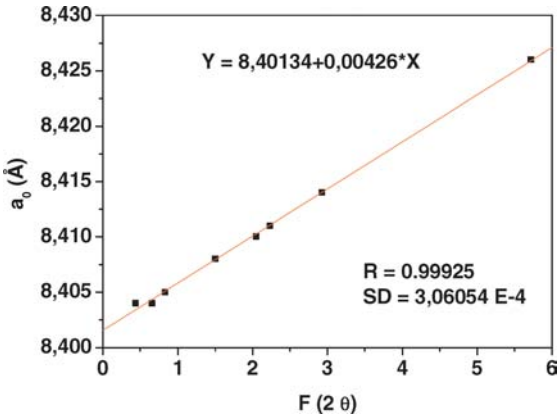

Figure 3 Extrapolation curve of lattice parameter a_0 of magnetite crystals.

Considering the calculation error, this value is quite closed to the crystallografic reference data (8.3985 Å).

The calibration curve for the quantitative analysis of magnetite using fluorite as internal standard is represented in Fig. 4. The correlation coefficient is $R = 0.99971$ and the standard deviation is SD = 0.13865. These statistical parameters suggest a very good fitting of the calibration curve. I(M)/I(F) represents the intensity ratio between the intensities of (311) magnetite diffraction line and (111) fluorite line. The quantity of magnetite crystallised in the glass-ceramic corresponds to 45 wt%. This quantity represents the stoichiometric amount of iron oxide in the material. So we can reasonably suppose that all the iron ions are contained in crystallised magnetite.

The second method utilised for the determination of the quantity of crystalline magnetite in the sample uses the Rietveld method for the profile fitting. First of all, the spectra of pure amorphous phase and pure magnetite were refined in order to obtain the available structure models. The silica glass model presented in the software was modified in order to achieve a good fitting of our amorphous structure. A polynomial background model was used for all spectra.

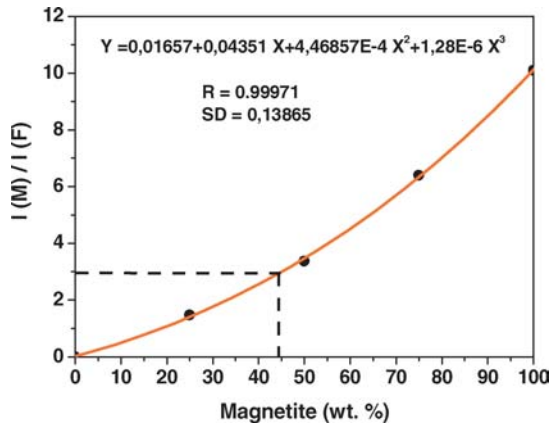

Figure 4 Calibration curve for quantitative analysis of magnetite (M) using fluorite (S) as internal standard.

TABLE V Crystal structure of magnetite estimated from XRD pattern, using the two programs

Magnetite parameters	X'Pert HighScore	MAUD
Crystals size d (nm)	53 ± 9	55 ± 0.5
Lattice constant a_o (Å)	8.4013 ± 0.0003	8.4019 ± 0.0004
Quantity of magnetite wt%	44.8 ± 0.1 (internal standard)	44.7 ± 0.2

The spectrum of the glass-ceramic was refined. The whole pattern profile fitting for the glass-ceramic is shown in Fig. 5. Differences between the two intensities are plotted at the bottom of the diagram. Vertical bars are the reflection position markers for magnetite and glass matrix. The fitting parameters: standard deviation ($\sigma = 1.82$), weighted sum of squares ($W_{ss} = 9068$) and the weighted correlation coefficient ($R_w = 10.3\%$) suggest a good fitting. An average crystal size of 55 nm, a cell length value of 8.402 Åand a quantity of 45 wt% of magnetite were estimated after refining.

The magnetite crystal structure data obtained by using the two methods (internal standard and Rietveld method) are illustrated comparatively in Table V. It can be seen that the resulted data are very similar.

3.2. Scanning electron microscopy

Fig. 6 shows the SEM micrographs of the etched surface of the glass-ceramic. Straight interpenetrated columns containing small different size crystals can be observed. Also, it can be clearly seen that each crystal has an octahedral shape, characteristic for a phase with a cubic structure. Magnetite is a typical cubic phase. These small crystals with octahedral morphology are identified as an iron oxide by EDS analysis. The small columns are uniformly distributed in the matrix. The mean size of the magnetite crystals is smaller than 0.5 μm.

3.3. Transmission electron microscopy

The TEM micrographs of glass-ceramic are shown in Fig. 7. Small dark particles embedded in the amorphous phase can be seen (see arrows). The particles present a large distribution in the range of about 5–10 nm.

Fig. 8 shows the selected area electron diffraction patterns of glass-ceramic particles. The particles are identified as magnetite from electron diffraction pattern. The diffraction signals related to (4 0 0), (4 2 2), (4 4 4), (6 4 2) and (7 3 1) planes were identified.

The halo due to the amorphous phase overlaps the signal related to the carbon film of the microgrid, so it is not possible to distinguish the two phases. On the other hand, by utilising copper uncoated microgrids, all the particles pass through the mesh and no particles deposition was observed.

The differences between the XRD, SEM and TEM measurement data are related to the sample preparation.

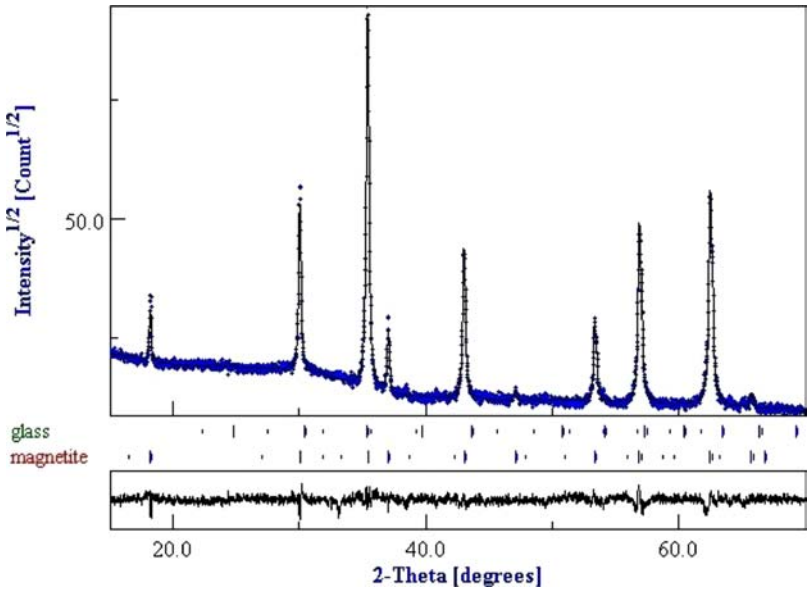

Figure 5 Whole pattern profile fitting for glass-ceramic S45 using the MAUD program.

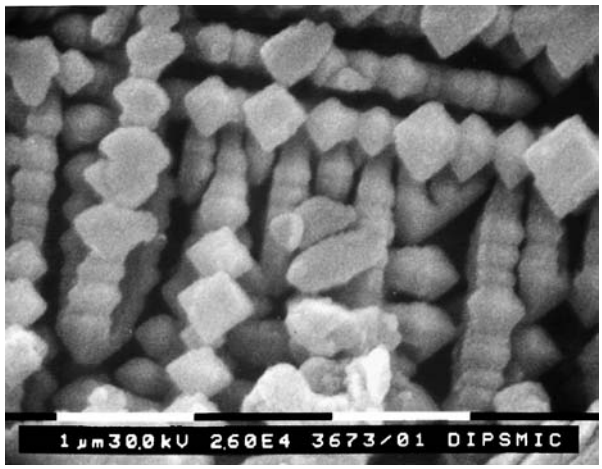

Figure 6 SEM micrograph of glass-ceramic S45 after etching.

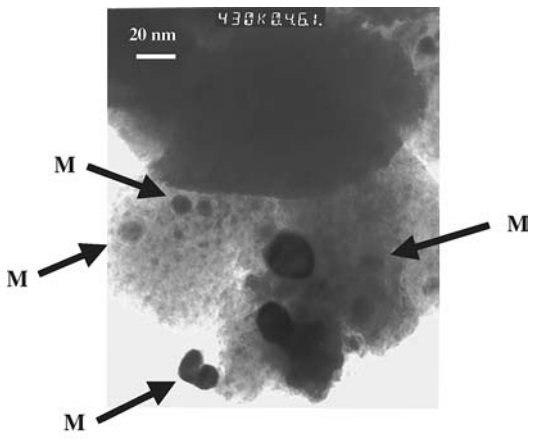

Figure 7 TEM micrograph of glass-ceramic S45 (magnification 430 × 10^3). M represents magnetite particles.

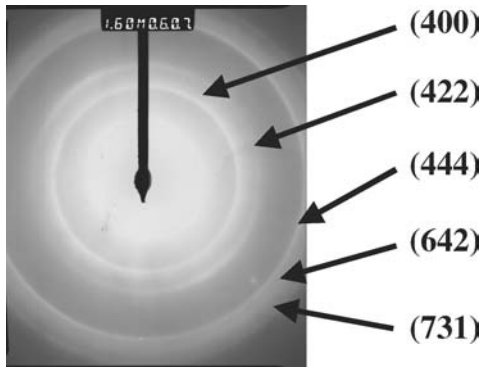

Figure 8 Selected area electron diffraction patterns of glass-ceramic S45.

For XRD and TEM analyses, micrometric powders (<45 μm) were employed, whereas for SEM analysis, small pieces of 50 mm^3 were utilised. SEM image shows the presence of many columnar aggregates, formed by teens of submicrometric magnetite crystals. XRD methods calculate the average volume relative of clusters of small crystals (in this case the average volume of one column of magnetite), while TEM image gives information about the shape and dimension of one crystal.

3.4. Magnetic measurements

The hysteresis loops for both magnetite and glass-ceramic sample under a magnetic field of 796 kA/m (10 kOe) are shown in Fig. 9. It can be seen that the two materials exhibit similar magnetic behaviour, characteristic of soft magnetic materials, with narrow hysteresis cycle and small coercive field. On the right bottom part of the Fig. 9 is presented a zoom-in plot of the central part of the hysteresis loop, in order to emphasise the coercive field.

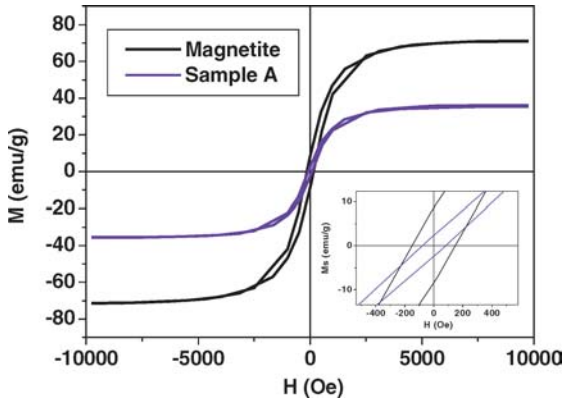

Figure 9 Room temperature hysteresis cycle up to 10 kOe for glass-ceramic S45 and magnetite.

The glass-ceramic has a saturation magnetisation of 34 A·m^2/kg (34 emu/g), and a coercive force of 6.8 kA/m (85 Oe). It saturates at a maximum field of 318 kA/m (4 kOe) and has a remanence magnetisation of 2.4A · m^2/kg (2.4 emu/g)

The saturation magnetisation Ms of magnetite particles is around 72A · m^2/kg (72 emu/g), which is lower than magnetic data reported on magnetite (Ms = 92 emu/g) [21]. This fact can be accounted considering that the measured samples are powders. As a consequence, they have a much larger surface/volume ratio than bulk materials whose saturation magnetisation is reported in literature. Surface effects can modify the saturation magnetisation of a magnetic material (usually lowering the magnetisation). The coercive force of magnetite is around 12 kA/m (150 Oe) and is between the reported limits.

The saturation magnetisation of the crystals depends almost linearly on the content of the magnetite. This means that the quantity of magnetite crystallised in the glass-ceramics can be calculated from the ratio between M_S of the sample and M_S of the pure magnetite. The amount of magnetite crystals estimated in the sample is about 47 wt%. This value is in a good agreement with XRD data. It must be reminded that the maximum quantity of magnetite which is possible to be formed according to the chemical composition is 45 wt%. The reported results are summarised in Table VI.

In order to evaluate the area of hysteresis cycle, we integrated the loop area of sample, extrapolating between ±796 kA/m (±10 kOe). The hysteresis area is around 1.45 mJ/g (14.5 kerg/g).

Such intense magnetic field is difficult to be applied in a hospital due to technical problems for construction of magnetic field generator. Therefore, room temperature hysteresis cycles were also performed at much lower field amplitude. Magnetic hysteresis cycles of glass-ceramic measured at 39.8 kA/m (500 Oe) and 4.8 kA/m (60 Oe) are shown in Fig. 10. It can be clearly seen that the loop area decreases drastically with magnetic field. The values

TABLE VI Magnetic parameters of glass-ceramic S45 estimated from hysteresis cycle

Magnetic parameters	SI units	CGS units
Saturation magnetisation Ms	34A·m^2/kg	34 emu/g
Remanence magnetisation Mr	2.4 A· m^2/kg	2.4 emu/g
Coercitive force Hc	6.8 kA/m	85 Oe
Maximum field saturation	318.4 kA/m	4 kOe
Magnetite quantity	47 wt%	47 wt%
Hysteresis area ± 10 kOe (±796 kA/m)	1.45 mJ/g	14500 erg/g
Hysteresis area ± 500 Oe (±39.8 kA/m)	0.17 mJ/g	1700 erg/g
Hysteresis area ± 60 Oe (±4.8 kA/m)	0.0015 mJ/g	15 erg/g

of hysteresis areas reported in Table VI are plotted in Fig. 11.

All the hysteresis cycles were measured in static conditions (frequency $f = 0$). Therefore, the area of the hysteresis loop represents the specific static loss/cycle. In dynamic conditions ($f > 0$), this area increases with augmentation of the frequency. Also, at high frequencies, the contribution of eddy currents loss is significant [21–23]. The total power loss obtained under dynamic conditions

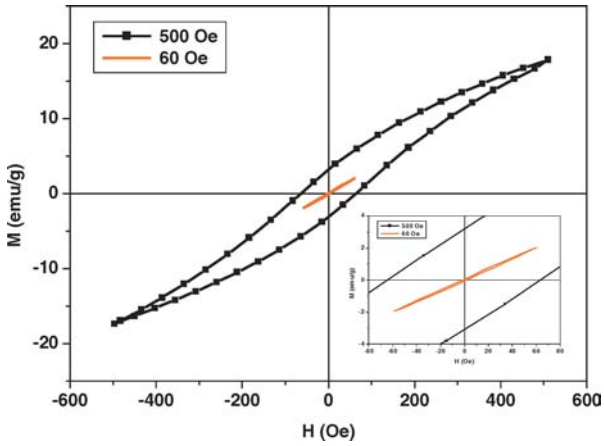

Figure 10 Room temperature hysteresis cycle at 500 and 60 Oe.

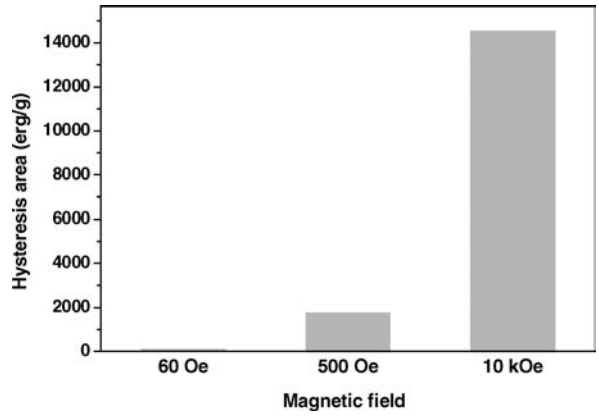

Figure 11 Variation of hysteresis area in function of the applied magnetic field for glass-ceramic S45.

is transformed in thermal energy. Using calorimetric data, we can estimate this heat generation under an alternating magnetic field with specific characteristics.

3.5. Calorimetric measurements

The specific power loss of glass-ceramic samples is determined from calorimetric data. A small piece of glass-ceramic (70 mg) immersed in 20 ml of water produces an increasing of water temperature of 3°C in an alternating magnetic field. The estimated heat generation under a magnetic field of 40 kA/m and 440 kHz is around 25 W/g. Similar values of specific power loss are reported by other authors for magnetite fine particles [24]. If higher strengths of magnetic fields are available, the obtained value of specific power loss will increase. This specific power loss represents actually the thermal energy, which will generate the heating of the tumour tissues.

Considering these experimental conditions reported above, we can estimate that, if 1 gram of glass ceramic is implanted into a tumour, it could produce an increasing of the temperature of maximum 35°C, around the tumour. This temperature variation is influenced by the tissue characteristics (blood flow effect, tissue's density, type of the neoplasm).

3.6. Bioactivity test

The bioactivity of the glass-ceramic containing 45 wt% of magnetite in the glass matrix, prepared in this work, was evaluated *in vitro* by examining the formation of bone-like apatite on its surfaces in SBF.

SEM micrograph of the surface of the glass-ceramic after soaking in SBF for 14 days is presented in Fig. 12a. The morphology of the hydroxylapatite crystals is shown in Fig. 12b, which illustrates a higher magnification of the marked area. The globular shape of the crystal aggregates, characteristic of precipitated hydroxylapatite [25], can be clearly seen. EDS analyses performed on an area of about 10 μm^2 of this sample, before and after soaking in SBF, are illustrated in Fig. 13. Before immersing in SBF, the characteristics peaks of sodium, calcium, silicon, phosphorus and iron (all the elements of the glass-ceramic) are clearly seen (Fig. 13a). Sodium ion is rather difficult to be detected since is often under-evaluated by the instrument.

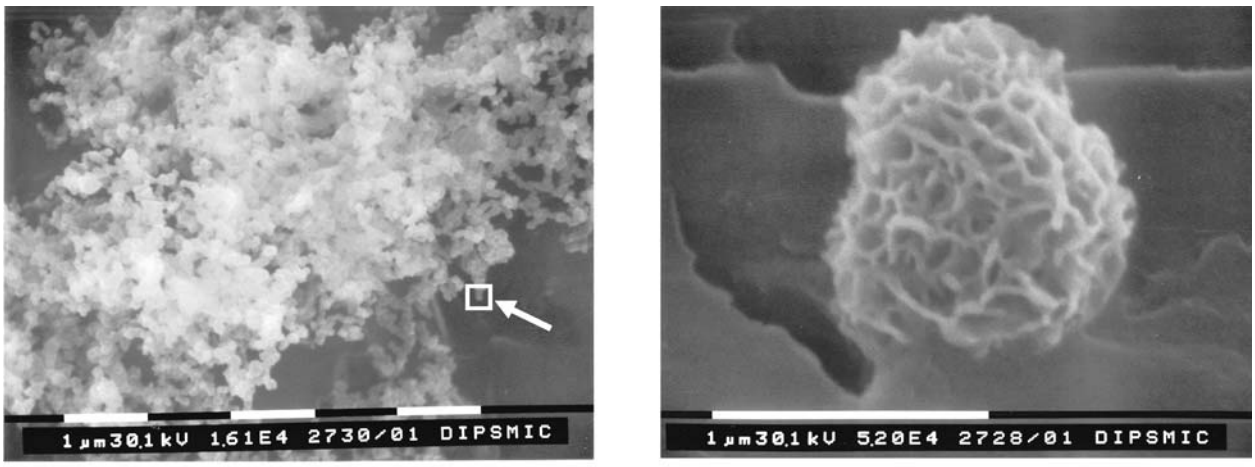

(a) (b)

Figure 12 (a) SEM micrograph of the surface of glass-ceramic S45 after soaking in SBF for 14 days and (b) a detail of the marked area.

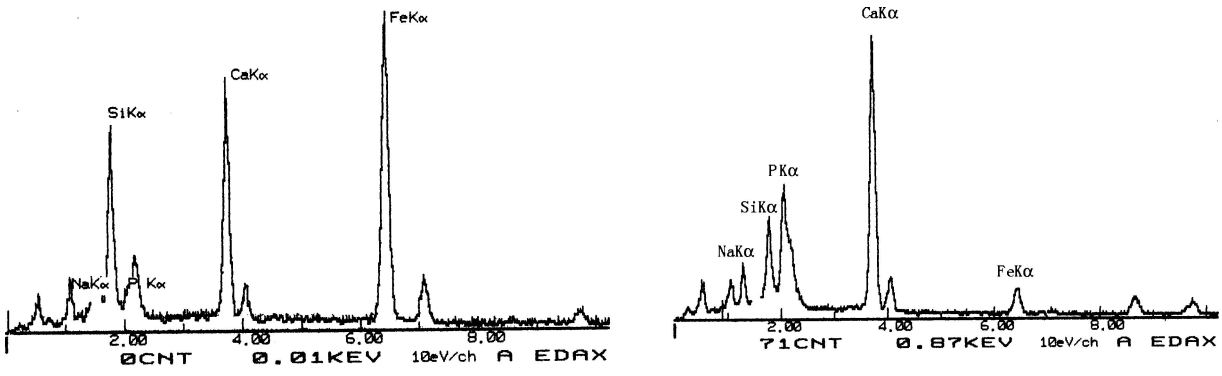

(a) (b)

Figure 13 Corresponding regional EDS analysis of the surface presented in the previous figure (a) before and (b) after soaking in SBF for 14 days.

After soaking in SBF, the predominant elements detected on the surface are calcium and phosphorus (Fig. 13b). Small quantities of iron and silicon are still presented in the glass-ceramic sample. The atomic ratio between Ca and P is close to the right Ca/P ratio of hydroxylapatite (1.67). Therefore, after soaking for 14 days in SBF, a layer of precipitated hydroxylapatite is formed. The layer rich in Ca and P was not detected by XRD analysis due to its low thikness.

4. Conclusions

In this study, a bioactive and ferrimagnetic glass-ceramic that contains a unique magnetic crystalline phase (magnetite crystals) in a glass matrix was synthesised. The referred glass-ceramic, with the composition in the system Na_2O–CaO–SiO_2–P_2O_5–FeO–Fe_2O_3, can be obtained by melting and quenching of coprecipitation-derived starting products. This glass-ceramic contains 45 wt% magnetite, which is produced during cooling from melting temperature to room temperature. No other subsequently nucleation and crystallisation treatments are necessary.

The magnetite crystals have dimensions of about 50 nm and are homogeneously distributed in the matrix.

The estimated heat generation of this glass-ceramic under the magnetic field of 40 kA/m and frequency of 440 kHz is 25 W/g.

After two weeks of immersion in SBF, a layer of precipitated hydroxylapatite is formed, so a bioactive behaviour was demonstrated.

The as obtained bioactive and ferrimagnetic glass ceramic could be a potential candidate for hyperthermic treatment of solid tumours, with a wider applicability due to its bioactive properties, for example for bone tumours.

The analysis of the influence of chemical composition and process parameters on the magnetic properties are in progress. The comparison between the coprecipitation-derived ferrimagnetic glass-ceramic and the one made by traditional melting method will be presented in a future paper.

Acknowledgments

The magnetic measurements were carried out at the Materials Department of "National Electrotechnique Institute Galileo Ferraris", Torino, Italy. Authors thank Marco Cöisson, Paola Tiberto, Paolo Allia and Franco Vinai for their helpful assistance and discussion.

The calorimetric measurements were performed at Manfredi S.p.A, Pinerolo, Italy. We are grateful to Eng. Roberto Agù and Giorgio Manfredi for their support.

References

1. G. H. NUSSBAUM, "Physical Aspects of Hyperthermia" (American Institute of Physics, Inc., 1982).
2. B. N. GRAY and S. K. JONES, "Targeted Hysteresis hyperthermia as a method for treating diseased tissue", U. S. Patent 6167313 (2000).
3. W. CAO and L. L. HENCH, *Ceram. Int.* **22** (1996) 493.
4. BORRELLI *et al.*, "Radio frequency induced hyperthermia for tumor therapy", U.S. Patent 4323056 (1982).
5. Y. K. LEE and S. Y. CHOI, *J. Amer. Ceram. Soc.* **79** (1996) 992.
6. S. H. OH, S. Y. CHOI, Y. K. LEE and K. N. KIM, *J. Biomed. Mater. Res.* **54** (2001) 360.
7. Y. EBISAWA, F. MIYAJI, T. KOKUBO, K. OHURA and T. NAKAMURA, *J. Ceram. Soc. Jpn.* **105** (1997) 947.
8. Y. EBISAWA, Y. SUGIMOTO, T. HAYASHI, T. KOKUBO, K. OHURA and T. YAMAMURO, *Sermikkusu Ronbunshi* **1** (1991) 7.
9. Y. EBISAWA, F. MIYAJI, T. KOKUBO, K. OHURA and T. NAKAMURA, *Biomaterials* **18** (1997) 1277.
10. M. FERRARIS, O. BRETCANU and E. VERNÉ, "Biocompatible magnetic materials for hyperthermia cancer treatment and their synthesis processing", Italian Patent IT2002TO00994 (2002).
11. O. BRETCANU, Ph.D thesis: "Magnetic Biomaterials for Hyperthermic Treatment of Cancer" (Politecnico di Torino, Italy, 2004).
12. H. KLUG and L. ALEXANDER, "X-ray Diffraction Procedures for Polycrystalline and Amorphous Materials" (John Wiley & Sons, Inc., London, 1962).
13. R. A. YOUNG, "The Rietveld Method" (IUCr, Oxford University Press, Oxford, UK, 1993).
14. A. LE BAIL, *J. Non-Cryst. Sol.*, **183** (1995) 39.
15. L. LUTTEROTTI and P. SCARDI, *J. Appl. Cryst.* **23** (1990) 246.
16. http://www.ing.unitn.it/~luttero/Publications/EPDIC_V/silicate_glass.html
17. M. MA, Y. ZHANG, W. YU, H. Y. SHEN, H. Q. ZHANG, AND N. GU, *Coll. Surf. A: Physicochem. Eng. Aspects.* **212** (2003) 219.
18. T. KOKUBO, Protocol for preparing Simulated Body Fluid SBF, http://sung7.kuic.kyoto-u.ac.jp/others/SBF/SBF_E.html
19. S. R. JANASI, M. EMURA, F. J. G. LANDGRAF and D. RODRIGUES, *"The effects of synthesis variables on the magnetic properties of coprecipitated barium ferrite powders"*, *J. Magnet. Magnetic Mater.* **238** (2002) 168.
20. O. BRETCANU, E. VERNÉ, L. BORELLO and A. R. BOCCACCINI, *"Bioactivity of degradable polymer sutures coated with bioactive glass"*, *J. Mater. Sci.: Mater. Med.* **15** (2004) 893.
21. R. D. CULLITY, "Introduction to Magnetic Materials" (Addison-Wesley Publishing Company Inc., 1972).
22. F. FIORILLO, Introduzione ai materiali magnetici, Istituto Elettrotecnico Nazionale Galileo Ferrarsi, Torino, 2001.
23. E. GENOVA and A. GOBETTO, Appunti di ferromagnetismo: perdite nei materiali ferromagnetici, Istituto Elettrotecnico Nazionale Galileo Ferraris, Torino, 1984
24. R. HERGT, W. ANDRÄ, C. G. D'AMBLY, I. HILGER, W. A. KAISER, U. RICHTER and H. G. SCHMIDT, *IEEE Trans. Magnet.*, **34** (1998) 3745.
25. S. DI NUNZIO, C. VITALE BROVARONE, S. SPRIANO, D. MILANES, E. VERNE', V. BERGO, G. MAINA and P. SPINELLI, *J. Europ. Ceram. Soc.* **24** (2004) 935.

Received 25 October 2004
and accepted 27 May 2005